of 3 mm (Fig. 4; see also movie S4). In the figures, thin-film interference is used to show the evolution, by using the lamellae thickness η to solve the Fresnel equations that determine the constructive and destructive interference of reflected light. After draining for 6.4 s, a single bubble bursts, which causes a rapid collapse of the foam structure. Compared to the case in Fig. 3, in this example the typical bubble size is much larger, which makes a priori prediction of rupture events less predictable.

In this work, we have developed a multiscale model of the interplay between gas, liquid, and interface forces for a dry foam, permitting the study of the effects of fluid properties, topology, bubble shape, and distribution on drainage, rupture, and rearrangement. We demonstrated the model by analyzing cascading properties of bubble rupture together with large-scale hydrodynamics. Both the scale-separated model and the underlying numerical algorithms are general enough to allow extension of the physics at individual scales to include other phenomena, such as disjoining pressure, diffusive coarsening, and different types of surface rheology, including liquid-gas interfaces with mobile/stress-free boundary conditions, surface viscosity, evaporation dynamics, and heating. The multiscale modeling and numerical methodologies presented here suggest a wide variety of related applications, such as in plastic and metal foam formation.

References and Notes

1. D. L. Weaire, S. Hutzler, *The Physics of Foams* (Oxford Univ. Press, 2001).
2. J. C. Bird, R. de Ruiter, L. Courbin, H. A. Stone, *Nature* **465**, 759 (2010).
3. J. Plateau, *Statique expérimentale et théorique des liquides soumis aux seules forces moléculaires* (Gauthier-Villars, Trubner et cie., Paris, France, 1873).
4. D. L. Chopp, *J. Comput. Phys.* **106**, 77 (1993).
5. K. Polthier, *Global Theory of Minimal Surfaces, Proceedings of the Clay Mathematics Institute 2001 Summer School*, D. Hoffman, Ed. (American Mathematical Society, Providence, RI, 2005).
6. J. von Neumann, *Metal Interfaces*, C. Herring, Ed. (American Society for Metals, Cleveland, OH, 1952), pp. 108–110.
7. W. W. Mullins, *J. Appl. Phys.* **27**, 900 (1956).
8. R. D. MacPherson, D. J. Srolovitz, *Nature* **446**, 1053 (2007).
9. S. Hilgenfeldt, A. M. Kraynik, S. A. Koehler, H. A. Stone, *Phys. Rev. Lett.* **86**, 2685 (2001).
10. A. Oron, S. H. Davis, S. G. Bankoff, *Rev. Mod. Phys.* **69**, 931 (1997).
11. T. G. Myers, *SIAM Rev.* **40**, 441 (1998).
12. S. A. Koehler, S. Hilgenfeldt, H. A. Stone, *J. Colloid Interface Sci.* **276**, 420 (2004).
13. M. Durand, H. A. Stone, *Phys. Rev. Lett.* **97**, 226101 (2006).
14. R. I. Saye, J. A. Sethian, *Proc. Natl. Acad. Sci. U.S.A.* **108**, 19498 (2011).
15. R. I. Saye, J. A. Sethian, *J. Comput. Phys.* **231**, 6051 (2012).
16. Y. Kim, M.-C. Lai, C. S. Peskin, *J. Comput. Phys.* **229**, 5194 (2010).
17. K. Brakke, *Exp. Math.* **1**, 141 (1992).
18. J. U. Brackbill, D. B. Kothe, C. Zemach, *J. Comput. Phys.* **100**, 335 (1992).
19. See supplementary materials on *Science* Online.
20. C. J. W. Breward, P. D. Howell, *J. Fluid Mech.* **458**, 379 (2002).
21. P. D. Howell, H. A. Stone, *Eur. J. Appl. Math.* **16**, 569 (2005).
22. A. J. Chorin, *Math. Comput.* **22**, 745 (1968).
23. U. Kornek *et al.*, *New J. Phys.* **12**, 073031 (2010).

Acknowledgments: This research was supported in part by the Applied Mathematical Sciences subprogram of the Office of Energy Research, U.S. Department of Energy, under contract DE-AC02-05CH11231, by the Division of Mathematical Sciences of the NSF, and by National Cancer Institute U54CA143833. Some computations used the resources of the National Energy Research Scientific Computing Center, which is supported by the Office of Science of the U.S. Department of Energy under contract DE-AC02-05CH11231. J.A.S. was also supported by the Miller Foundation at University of California, Berkeley, and as an Einstein Visiting Fellow of the Einstein Foundation, Berlin. R.I.S. was also supported by an American Australian Association Sir Keith Murdoch Fellowship.

Supplementary Materials

www.sciencemag.org/cgi/content/full/340/6133/720/DC1
Materials and Methods
Supplementary Text
Figs. S1 to S5
Table S1
References (*24*–*27*)
Movies S1 to S4

24 September 2012; accepted 8 April 2013
10.1126/science.1230623

Spin-Optical Metamaterial Route to Spin-Controlled Photonics

Nir Shitrit, Igor Yulevich, Elhanan Maguid, Dror Ozeri, Dekel Veksler, Vladimir Kleiner, Erez Hasman*

Spin optics provides a route to control light, whereby the photon helicity (spin angular momentum) degeneracy is removed due to a geometric gradient onto a metasurface. The alliance of spin optics and metamaterials offers the dispersion engineering of a structured matter in a polarization helicity–dependent manner. We show that polarization-controlled optical modes of metamaterials arise where the spatial inversion symmetry is violated. The emerged spin-split dispersion of spontaneous emission originates from the spin-orbit interaction of light, generating a selection rule based on symmetry restrictions in a spin-optical metamaterial. The inversion asymmetric metasurface is obtained via anisotropic optical antenna patterns. This type of metamaterial provides a route for spin-controlled nanophotonic applications based on the design of the metasurface symmetry properties.

Metamaterials are artificial matter structured on a size scale generally smaller than the wavelength of external stimuli that enables a custom-tailored electromagnetic response of the medium and functionalities such as negative refraction (*1*), imaging without an intrinsic limit to resolution (*2*), invisibility cloaking (*3*), and giant chirality (*4*, *5*). An additional twist in this field originates from dispersion-engineered metamaterials (*6*, *7*). A peculiar route to modify the dispersion relation of an anisotropic inhomogeneous metamaterial is the spin-orbit interaction (SOI) of light; that is, a coupling of the intrinsic angular momentum (photon spin) and the extrinsic momentum (*8*–*10*). Consequently, the optical spin provides an additional degree of freedom in nanooptics for spin degeneracy removal phenomena such as the spin Hall effect of light (*9*, *11*–*14*). The chiral behavior originates from a geometric gradient associated with a closed loop traverse upon the Poincaré sphere generating the geometric Pancharatnam-Berry phase (*15*, *16*), not from the intrinsic local chirality of a meta-atom (*4*, *5*, *17*). Specifically, spin optics enables the design of a metamaterial with spin-controlled modes, as in the Rashba effect in solids (*18*–*21*).

The Rashba effect is a manifestation of the SOI under broken inversion symmetry [i.e., the inversion transformation $\mathbf{r} \rightarrow -\mathbf{r}$ does not preserve the structure ($\mathbf{r}$ is a position vector)], where the electron spin-degenerate parabolic bands split into dispersions with oppositely spin-polarized states. This effect can be illustrated via a relativistic electron in an asymmetric quantum well experiencing an effective magnetic field in its rest frame, induced by a perpendicular potential gradient ∇V, as represented by the spin-polarized momentum offset $\Delta k \propto \pm \nabla V$ (*18*–*21*). In terms of symmetries, the spin degeneracy associated with the spatial inversion symmetry is lifted due to a symmetry-breaking electric field normal to the heterointerface. Similar to the role of a potential gradient in the electronic Rashba effect, the space-variant orientation angle $\phi(x,y)$ of optical nanoantennas induces a spin-split dispersion of $\Delta k = \sigma \nabla \phi$ (*22*–*24*), where $\sigma_{\pm} = \pm 1$ is the photon spin corresponding to right and left circularly polarized light, respectively. We report on the design and fabrication of spin-optical metamaterial that gives rise to a spin-controlled dispersion due to the optical Rashba effect. The inversion asymmetry is obtained in artificial kagome structures with anisotropic achiral antenna configurations (Fig. 1, A and B) modeling the uniform ($q = 0$) and staggered ($\sqrt{3} \times \sqrt{3}$) chirality spin-folding modes in the kagome antiferromagnet (*25*–*27*). In the geometrically frustrated kagome lattice (KL), the reorder of the local magnetic moments transforms the lattice from an inversion symmetric (IS) to an inversion asymmetric (IaS) structure. Hence, we selected the KL as a platform for investigating the symmetry influence on spin-based manipulation of metamaterial dispersion.

It was previously shown that the localized mode resonance of an anisotropic void antenna

Micro and Nanooptics Laboratory, Faculty of Mechanical Engineering and Russell Berrie Nanotechnology Institute, Technion–Israel Institute of Technology, Haifa 32000, Israel.

*Corresponding author. E-mail: mehasman@technion.ac.il

is observed with a linear polarization excitation parallel to its minor axis (*14*, *23*). We used this anisotropy in artificial kagome structures, where the anisotropic antennas are geometrically arranged in such a way that their principal axes are aligned with the original spin direction in the magnetic KL phases. These metamaterials with the nearest-antenna distance of $L = 6.5$ μm were realized using standard photolithographic techniques (*24*) on a SiC substrate supporting resonant collective lattice vibrations [surface phonon polaritons (SPPs)] in the infrared region. We measured angle-resolved thermal emission spectra by a Fourier transform infrared spectrometer at varying polar and fixed azimuthal angles (θ,φ), respectively, while heating the samples to 773 K (see Fig. 1C for the experimental setup). The dispersion relation ω(k) at φ = 60° of the $q = 0$ structure (Fig. 1D) exhibits good agreement with the standard momentum-matching calculation (*28*) [see (*24*) for the isotropic KL analysis]. However, the measured dispersion of the $\sqrt{3} \times \sqrt{3}$ configuration (Fig. 1E) reveals new modes as a result of the inversion asymmetry of the structure, which may give rise to an optical spin degeneracy removal. By measuring the S_3 component of the Stokes vector representing the circular polarization portion within the emitted light (*24*, *29*), we observed the $\sqrt{3} \times \sqrt{3}$ spin-projected dispersion and found that the new modes yield a highly polarized emission with opposite spin states and a Rashba splitting of $\Delta k = 2\pi/3L$ (Fig. 1, F and G).

The removal of the spin degeneracy requires a spin-dependent correction to fulfill the momentum-matching equation. The spin-controlled dispersion of an IaS metamaterial obeys the spin-orbit momentum-matching (SOMM) condition $\mathbf{k}_e^{||}(\sigma) = \mathbf{k_{SPP}} + m\mathbf{G_1} + n\mathbf{G_2} - \sigma\mathbf{K_i}$, associated with two differentiated sets of reciprocal vectors: structural and orientational. Here, $(\mathbf{G_1}, \mathbf{G_2}) = \frac{\pi}{L}(\mathbf{x} + \mathbf{y}/\sqrt{3}, -\mathbf{x} + \mathbf{y}/\sqrt{3})$ are the structural reciprocal vectors determined by the $q = 0$ unit cell, whereas $\mathbf{K_{1,2}} = \frac{\pi}{3L}(-\mathbf{x} \mp \sqrt{3}\mathbf{y})$ are the orientational reciprocal vectors determined by a $\sqrt{3} \times \sqrt{3}$ unit cell (Fig. 2A, inset), associated with the local field distribution; $\mathbf{k}_e^{||}$ is the wave vector of the emitted light in the surface plane; $\mathbf{k_{SPP}}$ is the SPP wave vector; (m,n) are the indices of the radiative modes; and $i \in \{1,2\}$ is the index of the specific spin-dependent geometric Rashba term. Note that in the vector equation the sign of the orientational term is determined by the spin. Moreover, the specific geometric Rashba correction is a result of an arbitrary orientational vector choice from $\mathbf{K_{1,2}}$; based on this choice, the secondary vector linearly depends on the primary $\mathbf{K_i}$ and both the structural vectors $\mathbf{G_{1,2}}$. Hence, the SOMM condition arises from the combined contributions of the structural and orientational lattices resembling the structural and magnetic unit cells in the kagome antiferromagnet; yet, this concept is general and can be tailored to metamaterials and metasurfaces (*30*). Considering low modes of (m,n) ∈ {0,±1}, we calculated the spin-dependent dispersions at φ = 0° and 60° (Fig. 2, A and B, respectively), confirming the S_3 measured dispersions (Fig. 1, F and G, respectively), with the optical Rashba spin split of $2\pi/3L$. Such a spin-split dispersion is due to a giant optical Rashba effect, as the geometric Rashba correction is in the order of magnitude of the structural term; in particular, the anomalous geometric phase gradient arising due to the space-variant antenna orientation in the investigated IaS photonic system resembles the potential gradient in the electronic Rashba effect.

The above condition can be also derived from symmetry restrictions, where the representation theory is applied to generate selection rules. If a given structure is invariant under a translation followed by a rotation and both operators commute, then a spin-orbit coupling is expected. By applying the representation theory formalism considering these symmetry constraints, a momentum selection rule with a spin-dependent geometric Rashba correction can be obtained. When this procedure is implemented for the $\sqrt{3} \times \sqrt{3}$ KL, which is invariant under a translation of $2L$ to the left followed by a rotation of 120° counterclockwise, the SOMM condition is realized [see (*24*) for the detailed discussion].

In addition to the spin-projected dispersions, selection rules can also specify the direction of the surface wave excited at a given frequency (Fig. 2, C to F). Hence, this concept serves as a platform for spin-controlled surface waves possessing excellent potential for manipulation on the nanoscale based on a geometric gradient. Particularly, the SOMM provides the basis for a new type of IaS spin-optical metamaterials, supporting spin-dependent plasmonic launching for nanocircuits (*31*, *32*) and multiport in on-chip photonics.

The observed optical Rashba spin-split dispersions reveal two obvious relations of (i) $\omega(k,\sigma_+) \neq \omega(k,\sigma_-)$, which is a signature of inversion symmetry violation, and (ii) $\omega(k,\sigma_+) = \omega(-k,\sigma_-)$, which is a manifestation of time reversal symmetry (Fig. 1, F and G, and Fig. 2, A and B). Moreover, the spin-projected dispersions show a clear discrimination between the different IaS directions, which is not observed in the degenerated intensity dispersions. By measuring the angle-resolved emission spectra at varying φ and fixed θ, we obtained the strength of the optical Rashba effect pointing on the IS and IaS directions in the KL (*24*). The S_3 dispersions of the $\sqrt{3} \times \sqrt{3}$ structure are shown in Fig. 3, A and B, where the time reversal symmetry is clearly seen; in addition, the IS directions of φ ∈ {30°,90°,150°} are manifested by the spin degeneracy, whereas in all other directions the degeneracy is removed.

The symmetry-based approach offers an extended condition because it also recognizes the IS directions resulting in spin-degenerated

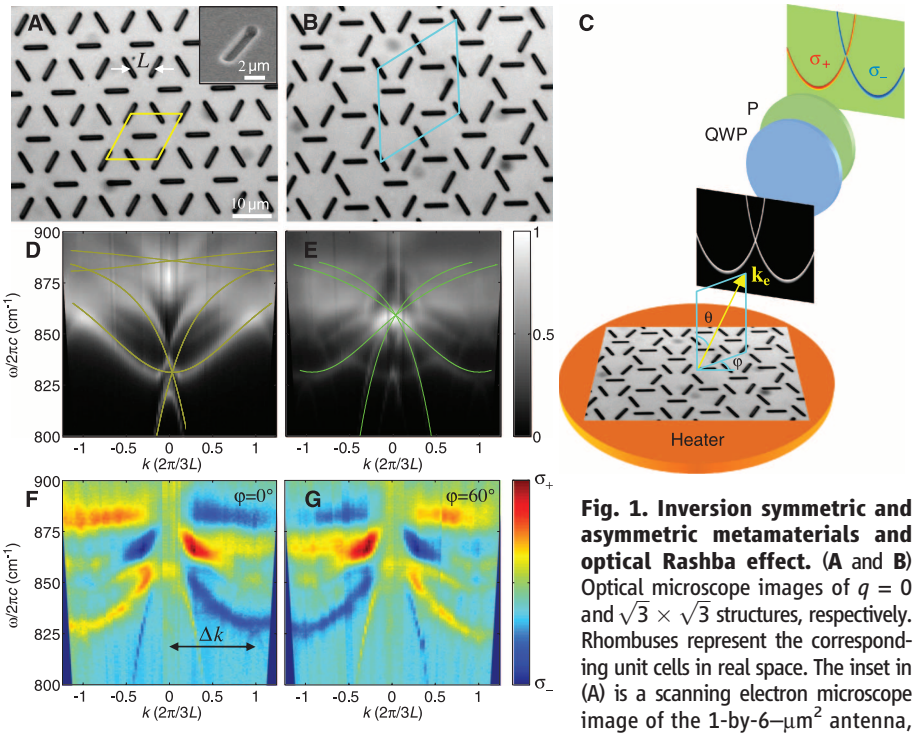

Fig. 1. Inversion symmetric and asymmetric metamaterials and optical Rashba effect. (**A** and **B**) Optical microscope images of $q = 0$ and $\sqrt{3} \times \sqrt{3}$ structures, respectively. Rhombuses represent the corresponding unit cells in real space. The inset in (**A**) is a scanning electron microscope image of the 1-by-6–μm^2 antenna, etched to a depth of 1 μm on a SiC substrate. (**C**) Schematic setup for the spin-projected dispersion based on the spin-optical metamaterial symmetry. The thermal radiation polarization state is resolved with the use of a circular polarization analyzer [a quarter-wave plate (QWP) followed by a linear polarizer (P)]. $\mathbf{k}_e$, wave vector of the emitted light. (**D** and **E**) Measured intensity dispersions of thermal emission from $q = 0$ and $\sqrt{3} \times \sqrt{3}$ structures, respectively. Yellow lines in (D) correspond to the standard momentum-matching calculation; green lines in (E) highlight the new modes. c, speed of light. (**F** and **G**) Measured spin-polarized dispersions of the $\sqrt{3} \times \sqrt{3}$ structure along the IaS directions of φ = 0° and 60°, respectively.

dispersions. As a reference, we measured the intensity dispersions of the $q = 0$ structure at $\varphi = 30°$, verifying the standard momentum-matching calculation without the geometric Rashba correction. Note that this direction is arbitrary because this structure is IS in all directions; however, it is a specific IS direction in the $\sqrt{3} \times \sqrt{3}$ structure. In accordance with this condition, we did not observe any spin dependence in the measured $\sqrt{3} \times \sqrt{3}$ spin-projected dispersion at this direction. This result is supported by the SOMM condition (Fig. 3D), which is general because it distinguishes between the IS and IaS directions and tailors a spin-degenerated or spin-dependent output, respectively, and it reveals new modes observed in the $\sqrt{3} \times \sqrt{3}$ intensity dispersion (Fig. 3C) owing to the spin-dependent geometric Rashba correction.

The spin degeneracy removal was also shown in the near-field associated with the orbital angular momentum variation along the IaS directions. We revealed a chain of vortices with alternating helicities in the artificial $\sqrt{3} \times \sqrt{3}$ building blocks, carrying a spin-dependent space-variant orbital angular momentum arising from the spiral phase front of the SPPs [see (*24*) for the detailed analysis]. The reported spin-based phenomena in the near- and far-fields inspire the development of a unified theory to establish a link between the spin-controlled radiative modes and the metasurface symmetry properties to encompass a broader class of metastructures from periodic to quasi-periodic or aperiodic. The design of metamaterial symmetries via geometric gradients provides a route for integrated nanoscale spintronic spin-optical devices based on spin-controlled manipulation of spontaneous emission, absorption, scattering, and surface-wave excitation.

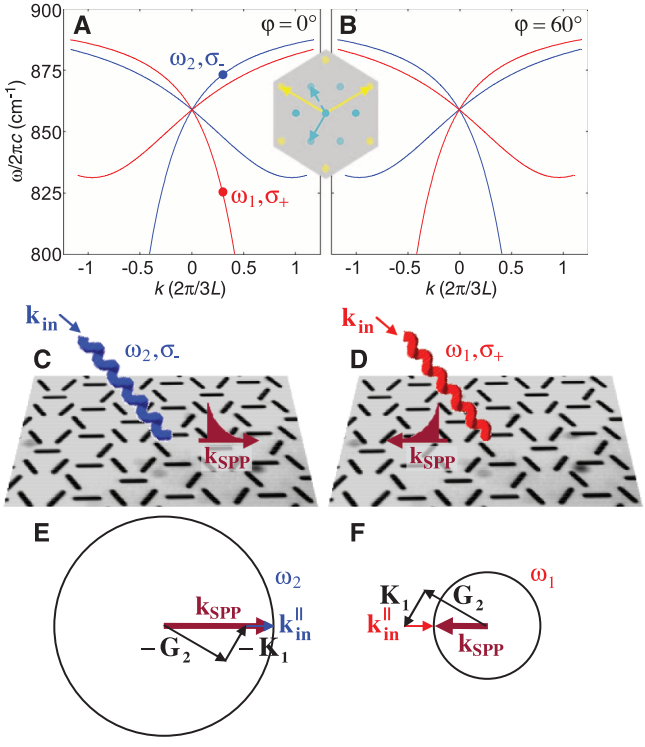

Fig. 2. Spin-orbit momentum-matching and surface-wave control. (**A** and **B**) Calculated S_3 dispersions of the $\sqrt{3} \times \sqrt{3}$ structure at φ = 0° and 60°, respectively, via the SOMM condition. Red and blue lines correspond to σ_+ and σ_- spin states, respectively. (Inset) Reciprocal space of $q = 0$ (yellow) and $\sqrt{3} \times \sqrt{3}$ (blue) structures with the corresponding reciprocal vectors. The dashed blue arrow indicates that only one of the $\sqrt{3} \times \sqrt{3}$ reciprocal vectors is required to set the dispersion of a spin-optical metamaterial, in addition to both of the $q = 0$ reciprocal vectors. (**C** and **D**) Spin-controlled surface-wave concept. The scheme introduces the coupling of the two spin-dependent modes depicted in (A) to surface-wave modes via the degree of freedoms of ω, $\mathbf{k}_{in}^{\parallel}$, and σ; $\mathbf{k}_{in}^{\parallel}$ is the component of the incident wave vector $\mathbf{k}_{in}$ parallel to the surface. (**E** and **F**) Vector summation representation of the SOMM condition forecasting the direction of the surface wave for the aforementioned modes.

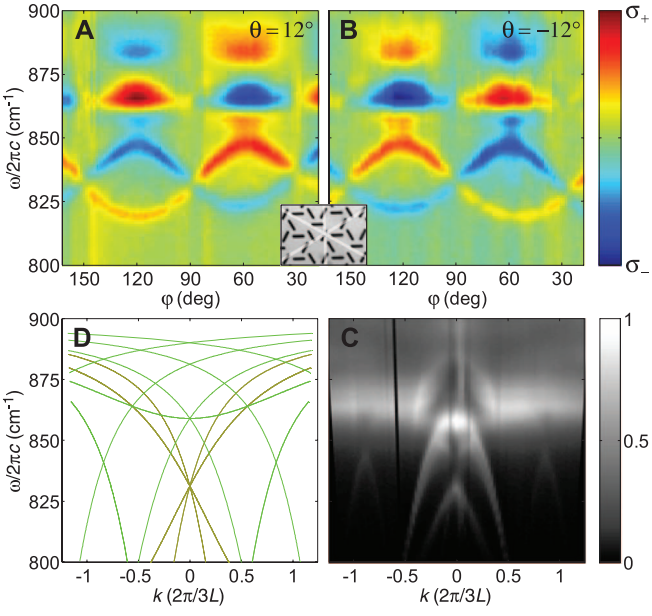

Fig. 3. Symmetry analysis by spin-projected measurements. (**A** and **B**) Measured S_3 dispersions of the $\sqrt{3} \times \sqrt{3}$ structure with varying φ at θ = 12° and –12°, respectively. The inset highlights the IS directions. (**C** and **D**) Measured and calculated intensity dispersions of the $\sqrt{3} \times \sqrt{3}$ structure along an IS direction of φ = 30°, respectively. The standard momentum-matching and the SOMM calculations in (D) are denoted by the yellow and green lines, respectively.

References and Notes

1. R. A. Shelby, D. R. Smith, S. Schultz, *Science* **292**, 77 (2001).
2. J. B. Pendry, *Phys. Rev. Lett.* **85**, 3966 (2000).
3. W. Cai, U. K. Chettiar, A. V. Kildishev, V. M. Shalaev, *Nat. Photonics* **1**, 224 (2007).
4. A. V. Rogacheva, V. A. Fedotov, A. S. Schwanecke, N. I. Zheludev, *Phys. Rev. Lett.* **97**, 177401 (2006).
5. S. Zhang *et al.*, *Phys. Rev. Lett.* **102**, 023901 (2009).
6. Z. Jacob, L. V. Alekseyev, E. Narimanov, *Opt. Express* **14**, 8247 (2006).
7. H. N. S. Krishnamoorthy, Z. Jacob, E. Narimanov, I. Kretzschmar, V. M. Menon, *Science* **336**, 205 (2012).
8. V. S. Liberman, B. Y. Zel'dovich, *Phys. Rev. A* **46**, 5199 (1992).
9. K. Y. Bliokh, Y. Gorodetski, V. Kleiner, E. Hasman, *Phys. Rev. Lett.* **101**, 030404 (2008).
10. N. M. Litchinitser, *Science* **337**, 1054 (2012).
11. O. Hosten, P. Kwiat, *Science* **319**, 787 (2008).
12. Y. Gorodetski, A. Niv, V. Kleiner, E. Hasman, *Phys. Rev. Lett.* **101**, 043903 (2008).
13. K. Y. Bliokh, A. Niv, V. Kleiner, E. Hasman, *Nat. Photonics* **2**, 748 (2008).
14. N. Shitrit, I. Bretner, Y. Gorodetski, V. Kleiner, E. Hasman, *Nano Lett.* **11**, 2038 (2011).
15. M. V. Berry, *J. Mod. Opt.* **34**, 1401 (1987).
16. Z. Bomzon, V. Kleiner, E. Hasman, *Opt. Lett.* **26**, 1424 (2001).
17. J. K. Gansel *et al.*, *Science* **325**, 1513 (2009).
18. G. Dresselhaus, *Phys. Rev.* **100**, 580 (1955).
19. E. I. Rashba, *Sov. Phys. Solid State* **2**, 1109 (1960).
20. K. Ishizaka *et al.*, *Nat. Mater.* **10**, 521 (2011).
21. P. D. C. King *et al.*, *Phys. Rev. Lett.* **107**, 096802 (2011).
22. N. Dahan, Y. Gorodetski, K. Frischwasser, V. Kleiner, E. Hasman, *Phys. Rev. Lett.* **105**, 136402 (2010).
23. K. Frischwasser, I. Yulevich, V. Kleiner, E. Hasman, *Opt. Express* **19**, 23475 (2011).
24. See supplementary materials on *Science* Online.
25. D. Grohol *et al.*, *Nat. Mater.* **4**, 323 (2005).
26. R. Moessner, A. P. Ramirez, *Phys. Today* **59**, 24 (2006).
27. W. Schweika, M. Valldor, P. Lemmens, *Phys. Rev. Lett.* **98**, 067201 (2007).
28. T. W. Ebbesen, H. J. Lezec, H. F. Ghaemi, T. Thio, P. A. Wolff, *Nature* **391**, 667 (1998).
29. E. Collett, *Polarized Light: Fundamentals and Applications* (Marcel Dekker, New York, 1993).
30. N. Yu *et al.*, *Science* **334**, 333 (2011).
31. E. S. Barnard, R. A. Pala, M. L. Brongersma, *Nat. Nanotechnol.* **6**, 588 (2011).
32. A. Schiffrin *et al.*, *Nature* **493**, 70 (2013).

Acknowledgments: This research was supported by the Israel Science Foundation.

Supplementary Materials

www.sciencemag.org/cgi/content/full/340/6133/724/DC1
Materials and Methods
Supplementary Text
Figs. S1 to S6
References (*33*–*37*)

7 January 2013; accepted 13 March 2013
10.1126/science.1234892

Spin-Optical Metamaterial Route to Spin-Controlled Photonics
Nir Shitrit, Igor Yulevich, Elhanan Maguid, Dror Ozeri, Dekel Veksler, Vladimir Kleiner and Erez Hasman (May 9, 2013)
Science **340** (6133), 724-726. [doi: 10.1126/science.1234892]

Editor's Summary

Making Metamaterials

Controlling the propagation of electromagnetic waves is a key requirement in communication technologies. The components tend to be bulky, however, which can make it difficult to integrate with microelectronics circuits. Using arrays of metallic nanoantennae patterned on a substrate surface, **Shitrit *et al.*** (p. 724) fabricated a novel class of metamaterials: anisotropic materials without inversion symmetry. The materials may pave the way to polarization-dependent nanophotonics.

Science (print ISSN 0036-8075; online ISSN 1095-9203) is published weekly, except the last week in December, by the American Association for the Advancement of Science, 1200 New York Avenue NW, Washington, DC 20005.